Ocsoy, I., Gulbakan, B., Shukoor, M. I., Xiong, X., Chen, T., Powell, D. H. & Tan, W. Aptamer-conjugated multifunctional nanoflowers as a platform for targeting, capture, and detec...

ARTICLE *in* ACS NANO · DECEMBER 2012

Impact Factor: 12.88 · DOI: 10.1021/nn304458m · Source: PubMed

Aptamer-Conjugated Multifunctional Nanoflowers as a Platform for Targeting, Capture, and Detection in Laser Desorption Ionization Mass Spectrometry

Ismail Ocsoy,[†,§] Basri Gulbakan,[†,§] Mohammed Ibrahim Shukoor,[†] Xiangling Xiong,[†,‡] Tao Chen,[†] David H. Powell,[†] and Weihong Tan[†,‡,*]

[†]Center for Research at the Bio/Nano Interface, Department of Chemistry and Shands Cancer Center, UF Genetics Institute and McKnight Brain Institute, University of Florida, Gainesville, Florida 32611, United States and [‡]Molecular Science and Biomedicine Laboratory, State Key Laboratory of Chemo/Bio-Sensing and Chemometrics, College of Biology and College of Chemistry and Chemical Engineering, Hunan University, Changsha 410082, China. [§]These authors contributed equally to this work.

ABSTRACT

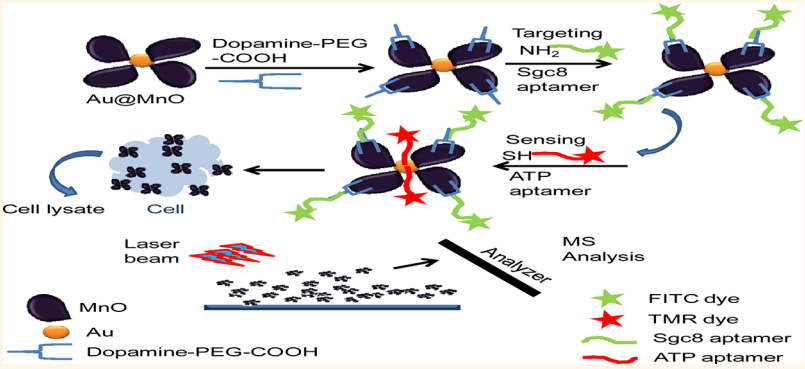

Although many different nanomaterials have been tested as substrates for laser desorption and ionization mass spectrometry (LDI-MS), this emerging field still requires more efficient multifuncional nanomaterials for targeting, enrichment, and detection. Here, we report the use of gold manganese oxide (Au@MnO) hybrid nanoflowers as an efficient matrix for LDI-MS. The nanoflowers were also functionalized with two different aptamers to target cancer cells and capture adenosine triphosphate (ATP). These nanoflowers were successfully used for metabolite extraction from cancer cell lysates. Thus, in one system, our multifunctional nanoflowers can (1) act as an ionization substrate for mass spectrometry, (2) target cancer cells, and (3) detect and analyze metabolites from cancer cells.

KEYWORDS: hybrid nanoparticles · nanoflower · aptamer · ATP · cancer cell · mass spectrometry

The size- and shape-dependent electronic, optical, and magnetic properties of colloidal nanomaterials, such as metallic nanoparticles or polymeric nanoparticles, are commonly used in a wide range of biomedical applications.[1−3] For example, various Ag, Au, or Cu plasmonic nanoparticles have been utilized for imaging, therapy, drug delivery, proteomics, and biosensing and surface plasmon resonance (SPR) purposes.[4−6] Various types of magnetic nanoparticles have been employed for immunoseparation, proteomics, magnetic drug delivery, and magnetic resonance imaging (MRI).[7,8]

Recently, multifunctional hybrid nanoparticles have attracted great attention because of their enhanced properties compared to their individual components and the possibility of multipurpose uses.[9,10] The high surface area provided by hybrid nanomaterials can simultaneously convey more than one functional group (*e.g.*, nucleic acids or aptamers, small chemical molecules,

* Address correspondence to tan@chem.ufl.edu.

Received for review September 26, 2012 and accepted December 4, 2012.

Published online
10.1021/nn304458m

antibodies, peptides) and/or carry multicancer drugs (water-soluble or insoluble) in cancer-specific delivery and/or combine several imaging agents (fluorescence dyes and radionuclides) for multimodal imaging. Particularly, multifunctional hybrid nanomaterials have been developed to overcome the limitations of conventional techniques used for diagnosis and therapy in biomedical applications.[11,12] For example, Fe_3O_4/MnO hybrid nanoparticles can be used for MRI, and the iron or manganese domain can be functionalized with targeting ligands to specifically recognize target cells. The cancer drugs or imaging agents can simultaneously be attached on the second domain of the same particles.[13,14] There are no significant interferences observed between functional groups on hybrid nanoparticles due to the presence of two discrete domains.[15,16]

These heterostructured materials composed of two or more different nanocomponents have been prepared in dumbbell, peanut, flower, and star shapes. For example, Sun and co-workers[17−19] developed and synthesized core−shell, dumbbell-like, and flower-shaped Au@Fe_3O_4 nanoparticles. These heterostructures have distinct advantages compared to individual Au and Fe_3O_4 nanoparticles. Their magnetic (Fe_3O_4) and optical (Au) active domains have been used, respectively, for magnetic imaging and optical detection purposes. Two-component dumbbell-like nanoparticles are also very suitable for selective immobilization of two different biofunctional groups for target capturing, imaging, and drug delivery. Chen *et al.*[20] and Tremel *et al.*[21] have, respectively, reported hybrid flower-like Au@Fe_3O_4 and Au@MnO nanoparticles which were used for simultaneous optical and MRI and therapy. In addition, gold nanostars with magnetic cores have been developed by Wei and co-workers[22] to demonstrate magnetomotive imaging by using the NIR scattering properties of the gold shell and the magnetic properties of the iron oxide cores. Thus, the limitations possessed by single-component NPs have been surpassed with development of hybrid NPs.

In addition to the aforementioned uses, NPs have recently been employed in a relatively new field called nanostructure-assisted laser desorption ionization mass spectrometry (nano-LDI). In parallel with the development of mass spectral instrumentation, such as tandem MS and imaging mass spectrometry, matrix-assisted laser desorption/ionization mass spectrometry (MALDI-MS) has become a well-established analytical tool for ionization and analysis of biomolecules. For instance, the prominent work was done by Deng and co-workers by using titanium dioxide decorated graphene composite (TiO_2/graphene) for the selective enrichment of phosphor from a mixture of peptide with matrix-assisted laser desorption ionization time-of-flight mass spectrometry (MALDI-TOF-MS).[23] However, signal suppression effects, shot-to-shot reproducibility problems, and the need for careful optimization of sample preparation still limit the use of MALDI-MS. Because the ionization process in MALDI is also very complex and still poorly understood,[24,25] progress in the development of new methods to improve ionization efficiency is slow.[25]

To overcome these problems, several nanomaterials have been developed and applied as matrices for laser desorption ionization mass spectrometry (LDI).[26] Essentially, the use of nanomaterials as energy-absorbing materials dates back to the early days of LDI development, in which ultrafine cobalt nanoparticles dispersed in glycerol were used to promote ionization.[27] However, because of the difficulty of handling glycerol and the resulting contamination in MS systems, the use of nanomaterials was largely overlooked until the development of desorption ionization on porous silicon (DIOS),[27] which initiated a new area called nanomaterial-based surface-assisted laser desorption/ionization. Following this seminal work, various nanomaterials have been tested as substrates for ionization, including plasmonic particles[28−33] (Au and Ag spheres and clusters), semiconductor crystals[34] (CdSe, CdS, and CdTe quantum dots), magnetic particles[35] (Fe_3O_4, CoO, and MnO), other metallic particles[36] (Pt and Pd), carbon-based materials[37] (SWCNTs, MWCNTs, GO, and combinations), and silicon wafers.[38] Chang and co-workers used the HgTe nanostructure as a new matrix to analyze protein, protein−drug complexes, and peptides as small biological molecules with the technique of surface-assisted laser desorption/ionization mass spectrometry (SALDI-MS).[39] HgTe nanostructure which was employed as a matrix provided high analyst signal and low background due to soft absorption and desorption process under the low laser power. The use of nanomaterials in MS has several additional advantages over organic matrices, including easy sample preparation, high salt tolerance, absence of self-ionization, and rapid data collection.[26]

While nanomaterials themselves are very useful as a matrix for ionization, their use as a tool to detect biomolecules in complex biological environments is difficult, as their intrinsic capturing ability is quite limited. So far, only a handful of examples exist in the literature where NPs were used both as a capturing probe and at the same time as an ionization matrix in a dual "catch and detect" format. This task can only be achieved by surface functionalization of nanoparticles. In the elegant approach of the Rotello group, the surfaces of Au NPs were functionalized with cationic ligands, and these "*mass barcodes*" were then used to assess the cellular uptake of Au NPs by LDI-MS.[29,40−42] This method has proven to be very successful in demonstrating the intracellular stability of NPs and excellent matrix properties of Au NPs for MS. The next best option is the use of tethering affinity ligand on NP surfaces. Siuzdak's group has demonstrated that

nanostructured DIOS surfaces can be selective by avidin−biotin chemistry[43] or through antibody immobilization.[44] Antibodies are very useful affinity probes; however, oriented chemical immobilization of them onto solid supports still represents a big hurdle. Generally, complex chemical strategies which deteriorate the antibody activity are needed.[45−48]

Aptamers have emerged as very attractive candidates for affinity tailoring of NP surfaces with enhanced recognition capabilities. Aptamers[49−51] are DNA- or RNA-based molecules selected by an *in vitro* iterative process called SELEX (systematic evolution of ligands by exponential enrichment). Aptamers can bind to their targets with high affinity and specificity and have been generated for a wide variety of targets, including small molecules[52,53] and ions,[54,55] large proteins,[56] and even biological cells.[49] Various different functional groups can easily be introduced onto aptamers without affecting their affinities. Therefore, aptamer surface immobilization onto NPs is quite easy and efficient compared to antibody immobilization. We and others have shown that aptamer-conjugated NPs can be used for specific cell targeting, rare protein capture and enrichment, drug delivery and therapy.[57−61]

Despite all of the efforts invested using NPs in MS applications, the choice of nanoparticles has largely been made by trial and error and very few studies have compared the performance of different nanoparticles for their performance for LDI-MS. However, on the basis of previous studies,[26,36] noble metals, such as Au and Pt nanoparticles, and metallic oxides have been reported to have better performance. It has also been reported very recently that bringing two nanostructures together results in better MS performance due to the synergistic effect.[62−64]

However, to the best of our knowledge, hybrid Au-metal oxide nanomaterials have not previously been tested for LDI-MS. Herein we report the use of a novel Au@MnO nanoflower-shaped nanoparticle matrix and compare its performance to similar, but differently shaped, nanoparticles, such as Fe_3O_4, Fe_3O_4@Au core/shell, Au-Fe_3O_4 dimer-like, and Au@Fe_3O_4 flower-like NPs (Supporting Information, Figure S2).

Furthermore, by using a benzyl pydridinium chloride thermometer ion, we have compared the survival yield of five different particles with different shapes and geometries, and we have demonstrated that Au@MnO nanoflowers serve as the matrix for LDI-MS among these particles (Supporting Information, Figures S3 and S4). After selecting Au@MnO nanoflowers as a material for ionization, we analyzed a series of different small molecules to show that this particle is indeed an efficient substrate for ionization which gives little or no background ions (Supporting Information, Figures S5−S8). Au@MnO nanoflowers were tested in the negative and positive ionization mode, as well as with model compounds, to show the proper mode for reduction of salt effects, which is important in the analysis of peptides, fatty acids, as well as nucleosides and nucleotides (Supporting Information, Figures S9 and S10).

The major goal of this study is to demonstrate the synergistic effect of two domains in one nanoflower particle for ionization and to also show how aptamers can improve the selectivity of this system. We have also functionalized the surfaces of Au@MnO nanoflowers to combine the selectivity of aptamers and the matrix capabilities of Au@MnO nanoparticles and used these as a proof of concept for selective isolation of ATP from cancer cells. Apart from its biological importance, ATP was chosen as a model target molecule for several reasons. First, a very good aptamer is already available for ATP targeting. Second, ATP is an abundant metabolite for MS analysis. Third, the molecular weight of ATP falls in the *m/z* range where nanoparticles show high ionization efficiency.[65]

RESULTS AND DISCUSSION

The aptamer-functionalized Au-MnO nanoflowers developed in this study can act as a targeting and sensing platform for selective metabolite extraction from cancer cell lysates followed by mass spectral analysis. The Au@MnO nanoflowers are functionalized with two different aptamers: sgc8 to target CCRF-CEM cancer cells and an anti-ATP aptamer to sense and capture ATP. Thus, in one system, these multifunctional Au@MnO nanoflowers can target cancer cells, capture metabolites, and serve as a mass spectrometry ionization substrate. The presence of two different domains, MnO and Au, simplified the surface modification and eliminated any interference between the two aptamers. Figure 1 shows that the synthesized Au@MnO nanoflowers were first made water-soluble using dopamine-PEG-COOH biopolymer. The dopamine side of the biopolymer has two hydroxyl groups that react with the MnO component of the nanoflowers through strong catechol reactions to transfer nanoflowers to an aqueous environment for bioapplications. To activate the carboxyl group of the biopolymer, EDC/NHS chemistry was applied to the dopamine-PEG-COOH biopolymer-attached nanoflowers. The amine (−NH_2)-group-terminated sgc8 aptamers were introduced into the activated dopamine-PEG-COOH nanoflower solution and incubated for 1 h. Secondary, thiol-modified anti-ATP aptamers were immobilized on the surface of the Au domain of nanoflowers through thiol−gold surface conjugation. Synthesis of the heterobifunctional ligand, dopamine-PEG-COOH, was carried out with the three following steps: (1) synthesis of 3,4-dihydroxyhydrocinnamic acid pentafluorophenol ester, (2) synthesis of NH_2-PEG-COOH, and (3) synthesis of dopamine-PEG-COOH (Supporting Information, Figure S1).

Au@MnO nanoflowers were characterized using TEM, HR-TEM, energy-dispersive X-ray (EDX) analysis, and UV—vis spectrometry. Figure 2 shows the TEM

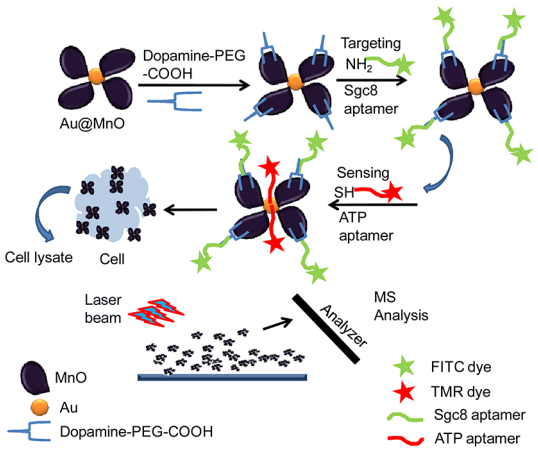

Sgc8: 5`–$NH_2$-ATC TAA CTG CTG CGC CGC CGG GAA AAT ACT GTA CGG TTA GA FITC–3`
ATP: 5`–SH ACC TGG GGG AGT ATT GCG GAG GAA GGT TMR–3`

Figure 1. Functionalization of nanoflowers. Schematic illustration of functionalization of Au@MnO nanoflowers with two different aptamers: FITC-labeled sgc8 (green) and TMR-labeled anti-ATP (red) for cell recognition and metabolite target sensing, respectively.

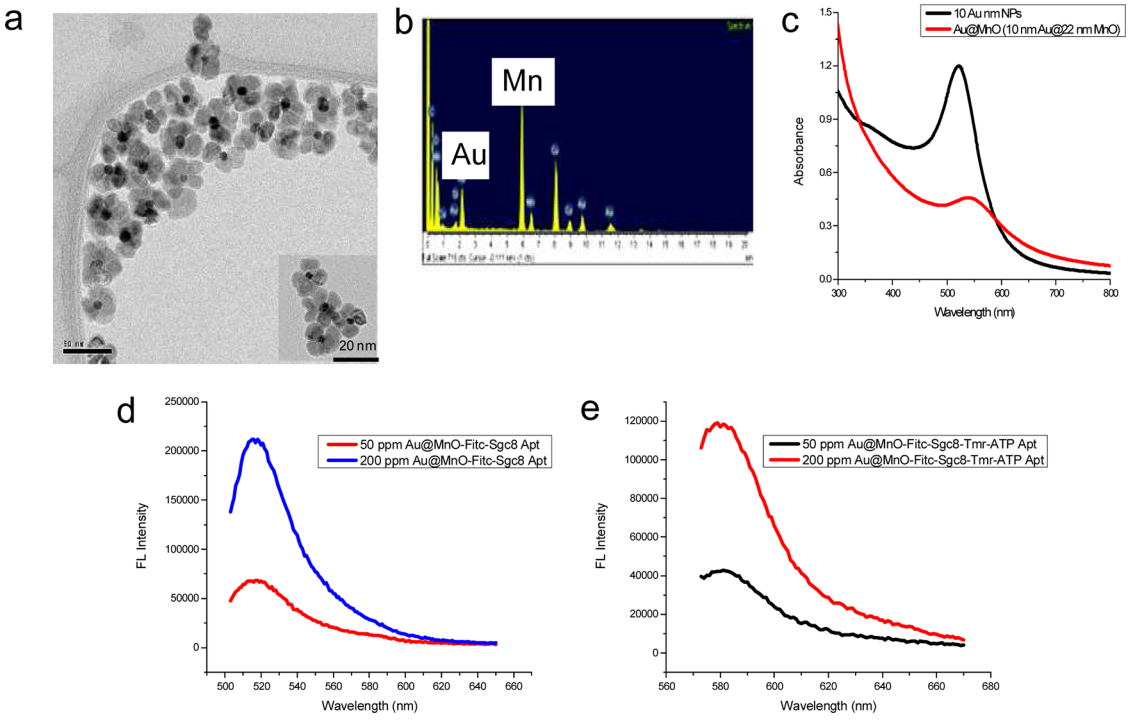

Figure 2. Characterization of Au@MnO nanoflowers and fluorophore-labeled aptamer binding. (a) TEM images of Au@MnO nanoflowers. Inset: HR-TEM image of nanoflowers. (b) Analysis of Au@MnO nanoflowers by dispersive X-ray spectroscopy (EDX). (c) UV/vis spectra of Au nanoparticles and Au@MnO nanoflowers. Fluorescence emission spectra of (d) FITC-labeled aptamer nanoflower conjugates (FITC: ex/em, 488 nm/520 nm) and (e) TMR-labeled aptamer nanoflowers (TMR: ex/em, 565 nm/580 nm) with two different concentrations of nanoflowers.

image of Au@MnO nanoflowers (Figure 2a) with large and discrete MnO petals by high-resolution transmission electron microscopy (HR-TEM) (inset). Several nucleation sites on the gold nanoparticles resulted in the formation of three or four MnO petals on Au seeds. The use of the optimum molar ratio (20:1) of the Mn-$(acac)_2$/Au$(OOCCH_3)_3$ precursors resulted in the absence of single Au or MnO NP formation. The MnO and Au elemental composition of nanoflowers can be observed on the EDX spectrum (Figure 2b). Au nanospheres exhibit a single and sharp absorption peak in the visible range between 505 and 560 nm based on size. In particular, Au nanospheres in the size range of 10−30 nm show a characteristic peak around 525 nm, which corresponds to the frequency of the surface plasmon oscillations. It is well-known that the position of the absorption peak of Au nanoparticles varies with shape, size, and surface coating, as well as the concentration of

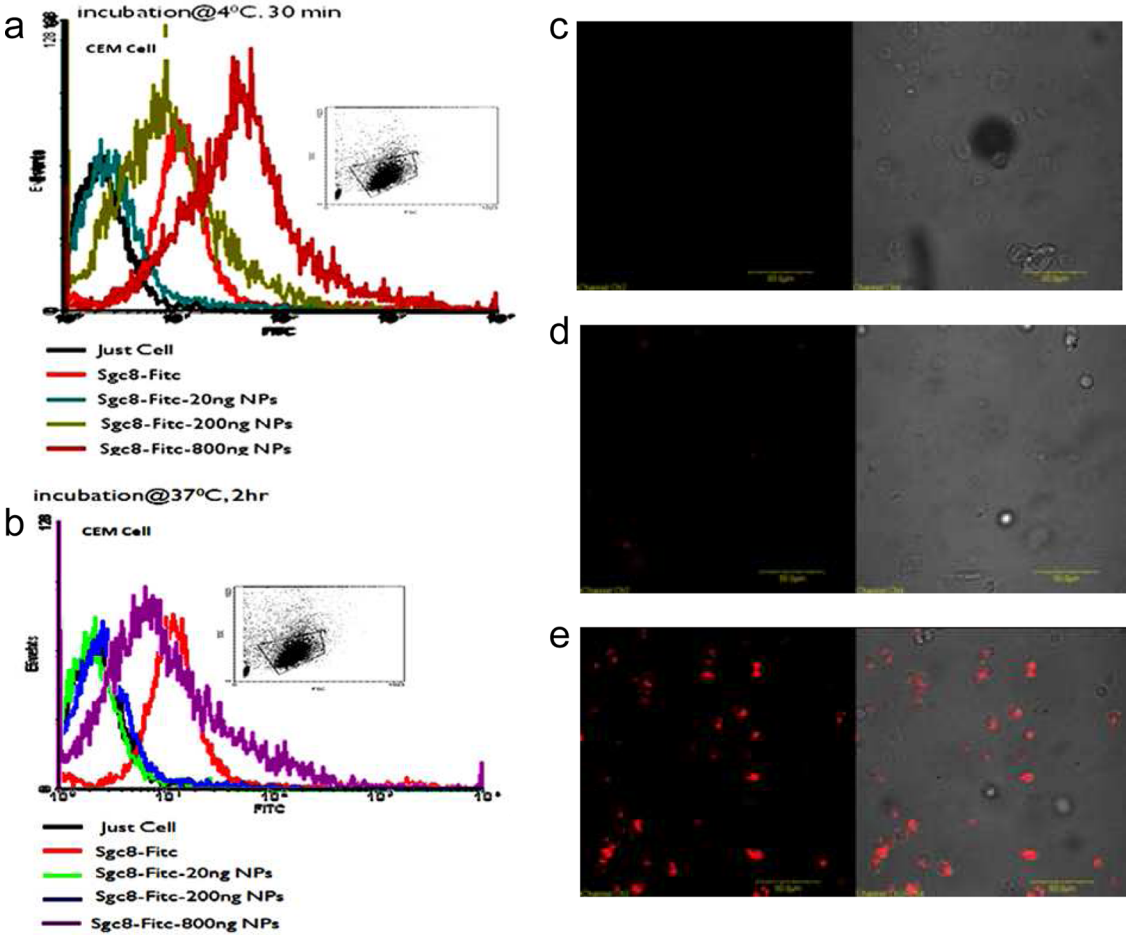

Figure 3. Flow cytometric analysis and *in vitro* confocal imaging. (a) Flow cytometric assay to monitor the binding of FITC-sgc8-conjugated nanoflowers (20, 200, 800 ng/mL) to CCRF-CEM cells (target cells) at 4 °C with 30 min incubation for surface binding and (b) at 37 °C, 2 h incubation for internalization. (c) Confocal microscopy images of cancer cells only. (d) Cancer cells incubated with bare nanoflowers without aptamer functionalization. (e) Cancer cells incubated at 37 °C for 2 h with aptamer-functionalized nanoflowers (800 ng).

other metals. Moreover, the nucleation of MnO petals on Au spheres creates an electron junction between the Au core and MnO petals and a high local dielectric effect around the Au core. Both effects lead to a remarkable red shift of wavelength to 565−580 nm and broadening of the peak (Figure 2c).

Figure 2d,e confirms that FITC-labeled sgc8 aptamer and TMR-labeled anti-ATP aptamer were successfully bound to the surface of the MnO and Au domains of nanoflowers, respectively. Figure 2d shows that the fluorescence intensity of FITC-labeled aptamers attached to the surface of MnO petals is enhanced with increasing numbers of nanoflowers. Because of the corresponding increase in the number of FITC-labeled sgc8 aptamers, TMR-labeled anti-ATP aptamers immobilized on nanoflower Au nanoparticles also exhibit higher fluorescence intensity with increasing numbers of nanoflowers (Figure 2d). No effective quenching was observed because the TMR-labeled ATP aptamers were not sufficiently close to the Au surface to initiate fluorescence resonance energy transfer (FRET), considering the length of the anti-ATP aptamer (29mers length with two end modifications, ∼10 nm) (Figure 2e). The effective FRET generally takes place in less than 10 nm distance, particular distance is ∼7 nm, between fluorophore and quencher or plasmonic NPs.[66] These two fluorescence spectra show that heterobiaptameric nanoflower conjugates can be prepared without significant interference between the aptamers.

Binding and internalization studies were performed at 4 and 37 °C, respectively. CCRF-CEM cells were prepared in six separate tubes and divided into two sets of three tubes each. One hundred microliters of 20, 200, and 800 ng/mL nanoflowers was added to each set. One set of tubes was incubated on ice at 4 °C for 30 min for a surface binding study, and the other set was incubated in an incubator shaker at 250 rpm (Thermo Electron Corporation, Forma Orbital Shaker Refrigerate, NC, USA) at 37 °C for 2 h for an internalization study. Figure 3a,b shows the flow cytometry results of the surface binding (Figure 3a) and internalization (Figure 3b). Two million CCRF-CEM cells were incubated with 20, 200, and 800 ng of sgc8 nanoflowers at 4 °C (surface binding) or at 37 °C (internalization). The nanoflowers (800 ng)

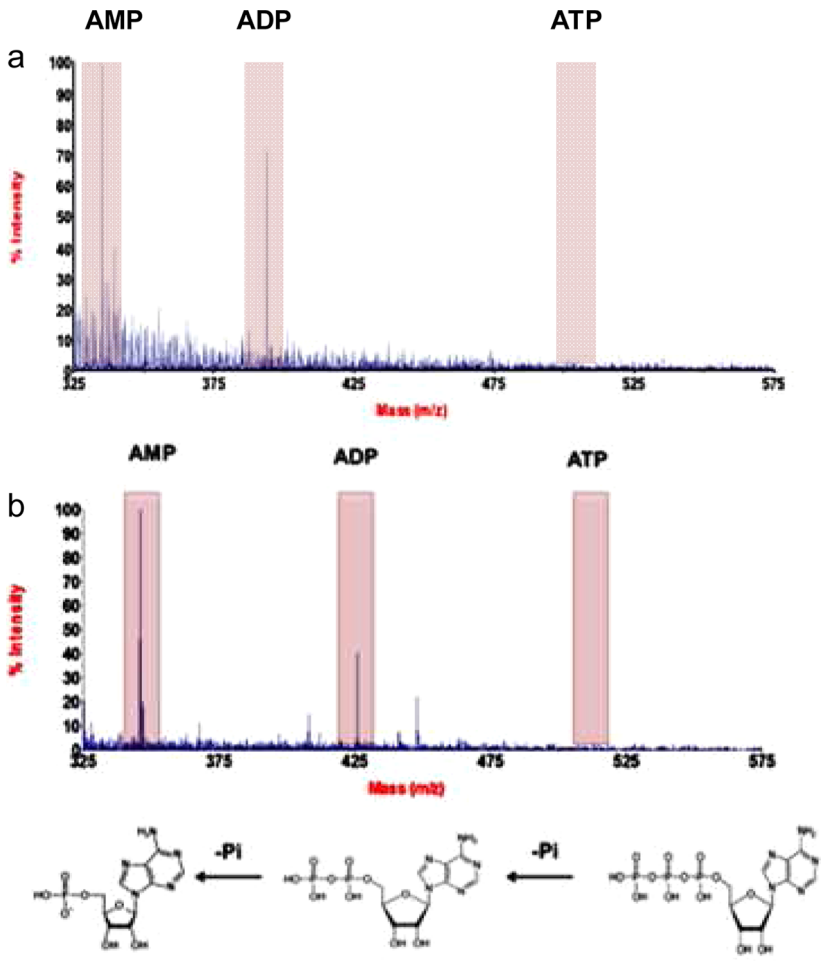

Figure 4. LDI-MS of CEM cell lysate after metabolite extraction: (a) with cold methanol using nanoflowers and (b) with hot water using nanoflowers.

showed optimum signal shift for surface binding and internalization in the flow cytometry experiment. A significant increase in the fluorescence signal occurred between the lowest (20 ng/mL) and highest (800 ng/mL) concentration of nanoflowers used for the cell uptake study. However, the fluorescent signal at 37 °C was lower than that reported at 4 °C, possibly because of particle aggregation in the cell, resulting in partial quenching of FITC dye, or the weak fluorescence nature of FITC dye attached to the sgc8 aptamer.

Cell internalization was verified by confocal microscopy utilizing the TMR label on the anti-ATP aptamer. Figure 3c,d shows no TMR fluorescence from the CCRF-CEM cells or cells incubated with bare nanoparticles. Cells incubated with TMR-labeled anti-ATP aptamer-functionalized nanoflowers (800 ng) displayed intense fluorescence signals (Figure 3e). The flow cytometry results of the surface binding and internalization using 800 ng/mL of nanoflowers are highly consistent with the confocal microscopy results.

After verification of nanoflower internalization, the next step was to test different cell lysis conditions to obtain the most efficient detection of metabolites by LDI-MS. Extraction of metabolites from cell lysates is an area of great interest, especially in the growing area of metabolomics.[67,68] In the past 5 years, several methods have been used with different conditions to release the metabolites from the biological mixtures,[69] but success still depends on trial- and error-based optimization. Organic solvents, such as cold acetone, methanol, and ethanol, have been generally used for metabolite extraction. In our first attempt, we used cold methanol for cell lysis. After treatment with cold methanol for 10 min, the final cell lysis mixture was brought to room temperature, and particles were centrifuged and removed from the cell lysate. After several cycles of washing, an aliquot of the particles was spotted onto the MALDI plate and analyzed. However, as shown in Figure 4a, no signal for ATP or its secondary metabolites could be observed. Lack of ATP signal could have resulted from (1) an insufficient amount of internalized particles and instability of the particles, (2) nonfunctional ATP aptamer within the cells because of cellular complexity or cleavage by endonucleases, or (3) disruption of aptamer–target interaction by cell lysis with organic solvents. The first two reasons are very unlikely because aptamers can be easily internalized and can recognize their targets, even in cells.[70–72]

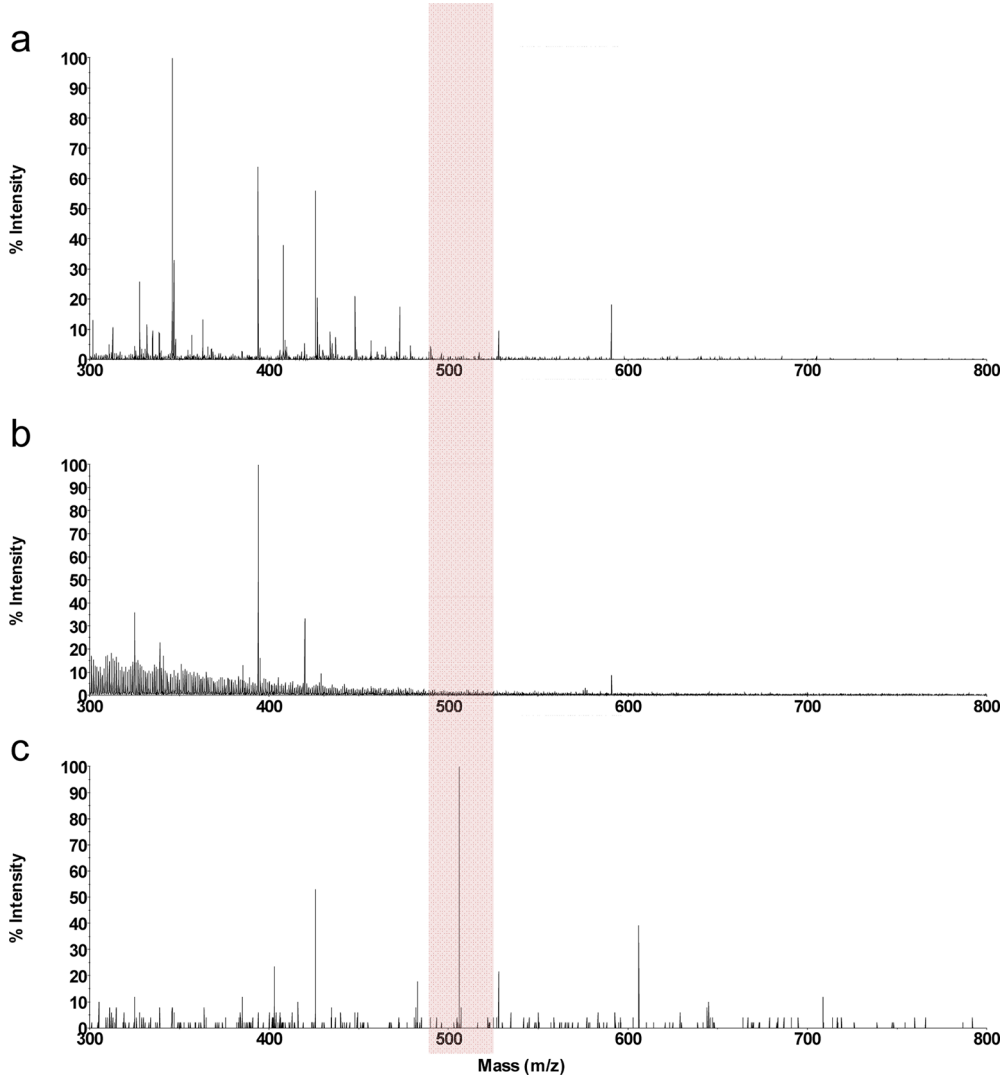

Figure 5. LDI-MS of CEM cell lysate after cell metabolite extraction with hot water followed by quenching with cold NH_4HCO_3 buffer and liquid N_2 to quench the metabolism. (a) Cell lysate and sgc8-conjugated nanoflowers. (b) Cell lysate and sgc8- and random DNA-conjugated nanoflowers. (c) Cell lysate and sgc8-ATP-conjugated nanoflowers.

Although it is possible that aptamers may be cleaved by cellular nucleases, recent studies showed that nanoparticles provide a strong barrier against such unwanted enzymatic reactions.[73] A notable example is the nanoflare method developed to monitor mRNA activity. This approach relies on immobilizing an oligonucleotide and a reporter complementary strand on a gold nanoparticle surface, then reporter complementary strand fluoresces upon target binding.[74] The authors showed that endonucleases did not cleave nanoparticle-immobilized oligonucleotides. This has also been demonstrated in a similar work on "aptamer nanoflares".[75] Moreover, by careful choice of the surface chemistry, recent studies have clearly demonstrated that gold nanoparticles are highly stable in cells. The last, and most likely, reason is the use of an organic solvent during cell lysis and metabolite extraction. Compared to antibodies, aptamers are more stable molecules against changes in pH, temperature, and ionic strength, but target recognition still depends on their 3D conformations. It is therefore very plausible that the cold methanol treatment irreversibly disrupts the aptamer–target interaction.

Therefore, in the next set of experiments, we replaced cold methanol with boiling water for metabolite extraction and cell lysis. While aptamers can be denatured with heat, they can easily refold to their proper 3D conformation upon cooling. Moreover, previous studies have shown that boiling water is a better solvent for extracting nucleotides from cells. We repeated the same experiments using water at 65 °C as the metabolite extraction solvent. However, this time we were challenged by the rapid turnover of ATP molecules to ADP and AMP. Because the anti-ATP aptamer also recognizes ADP and AMP, signals by these secondary metabolites were observed (Figure 4b).

To overcome this problem, we have slightly modified the metabolite extraction step by incorporating

another step using cold NH_4HCO_3 buffer and dipping the cells into liquid N_2 to quench the metabolism prior to metabolite extraction and cell lysis.[76] Using this method, the results in Figure 5 clearly show that ATP can be detected with no significant ATP decomposition. The respective control experiments show, to a great extent, that ATP can be captured, extracted, and detected only by the dual aptamer-modified Au@MnO nanoflowers.

CONCLUSIONS

In conclusion, our study demonstrated that flower-shaped Au@MnO nanoparticles could be efficiently used as a multifunctional platform to specifically target CCRF-CEM cells and capture ATP molecules from cell lysate. ATP as stated in our work was used as a model analyte, but potentially, this method can also be utilized for other intracellular targets where high affinity aptamers are available. The nanoflowers can also serve as an efficient ionization substrate for laser desorption/ionization without an additional matrix. Therefore, single-platform nanoflower conjugates containing MnO and Au components provide an ideal *all-in-one system* for selective functionalization with the desired biofunctional groups, as well as for use as an ionization substrate for LDI-MS.

EXPERIMENTAL SECTION

Chemicals and Materials. All chemicals were used as received without further purification. Manganese(II) acetylacetonate, $[Fe(CO)_5]$ 98%, oleic acid, oleylamine, 1-octadecene 90%, hexane, toluene >99%, 1,2,3,4-tetrahydronaphthalene 99%, *tert*-butylamine borane 97%, and phenyl ether 99% were obtained from Sigma-Aldrich. Gold(III) acetate >99.9% was purchased from Alfa Aesar. Hexane was purchased from Fisher. For the synthesis of dopamine-PEG-COOH, succinic anhydride, *N*,*N*-dicyclohexylcarbodiimide(DCC), 3,4-dihydroxyhydrocinnamic acid, and 3-(3,4-dihydroxyphenyl)propionic acid were obtained from Alfa Aesar. *O*,*O*-Bis(2-aminopropyl)polypropylene glycol-*block*-polyethylene glycol*block*-polypropyleneglycol-2,3,4,5,6-pentafluorophenol (PFP), 1,4-dioxane, and dithiothreitol (DTT) were purchased from Sigma-Aldrich.

Instrumentation and Characterization. One drop of Au@MnO nanoparticles dispersed in hexane was deposited on carbon-coated copper grids and allowed to dry for at least 2 h. Transmission electron microscopy (TEM) on a Hitachi H-7000 transmission electron microscope with a working voltage of 100 kV was used to obtain images of the nanoflowers. A JEOL JEM-2010F field emission electron microscope coupled with spatially resolved energy-dispersive X-ray spectroscopy (EDX) was also used for magnified images and further characterization of nanoflowers. An 1800 UV−vis spectrophotometer (Shimadzu Scientific Instruments, Columbia, MD) was used for the absorption spectra of nanoflowers and to determine the concentrations of DNA aptamers. Fluorescence measurements were carried out on a Fluoromax-4 (Horoba Jobin-Yvon, Edison, NJ, USA), which was also used for validation of the dye-labeled aptamer nanoflower conjugates. An Olympus FV-500-IX81 confocal microscope (Olympus, Center Valley, PA, USA) having a 40× oil-immersion objective was used to image cancer cells incubated with nanoparticles. Binding of functionalized nanoparticles to target cells was demonstrated with a FACScancytometer (Becton Dickinson Immunocytometry Systems, San Jose, CA, USA). All mass spectra were acquired using a MALDI-TOF/TOF mass spectrometer (ABI/SCIEX 5800, Applied Biosystems, Foster City, CA) with a Nd:YAG laser at 355 nm. The spectra were recorded in reflection mode in either positive or negative mode using an accelerating voltage of 20 kV, a 66% grid voltage, and a 50−200 ns delay extraction. Typically, 10−60 laser shots were collected per spectrum. Applied Biosystems Calibration Mixture 1 was used to calibrate the mass spectrometer. Data analysis was performed using Data Explorer software.

Cell Lines. CCRF-CEM cells (CCL-119 T-cell, human acute lymphoblastic leukemia) were obtained from ATCC (American Type Culture Collection). RPMI medium supplemented with 10% fetal bovine serum (FBS), and 100 IU/mL penicillin-streptomycin was used for cell culture (5% CO_2, 37 °C). A hemocytometer was used to determine the cell density before each experiment. Two million cells suspended in RPMI cell media were centrifuged at 970 rpm for 5 min and redispersed in 2 mL of washing buffer (Dulbecco's PBS with calcium chloride and magnesium chloride supplemented with 4.5 g/L glucose and 5 mM $MgCl_2$) for incubation.

Synthesis of Aptamers. An ABI3400 DNA/RNA synthesizer (Applied Biosystems, Foster City, CA) was used for the synthesis of the aptamers at the 1 μmol scale: TAMRA-modified aptamer sequences were deprotected in 0.05 M potassium carbonate in methanol at 65 °C for 3−4 h, and all other sequences were deprotected in AMA (ammonium hydroxide/40% aqueous methylamine 1:1) at 65 °C for 30 min. Deprotected sequences were purified by reversed-phase HPLC (ProStar-Varian, Walnut Creek, CA) with a C18 column (Econosil, 5 μm, 250−4.6 mm) from Alltech (Deerfield, IL) using the mixture of 100 mM triethylamine acetic acid buffer (TEAA, pH 7.5) and acetonitrile (0−30 min, 10−100%) as the mobile phase. After HPLC purification, the purified DNA solution was dried in acid-resistant centriVap centrifugal vacuum concentrators (Labconco, Kansas City, MO). The dried DNA was dissolved in 50 μL of DNA grade water, and the concentration of each sequence was determined based on the absorbance value at 260 nm using a UV-1800 UV−vis spectrophotometer (Shimadzu Scientific Instruments, Columbia, MD).

Synthesis of Au@MnO Nanoflowers. Au@MnO nanoparticles were synthesized using a modified method[21] with standard Schlenk line techniques. A solution containing diphenyl ether (10 mL), oleic acid (1 mL, 3 mmol), and oleylamine (2 mL, 4 mmol) was degassed at room temperature for 45 min and backfilled with argon at least three times to remove any trace of air and moisture. The degassed solution containing diphenyl ether (10 mL), oleic acid (1 mL, 3 mmol), and oleylamine (2 mL, 4 mmol) was injected into a 100 mL three-necked flask containing 1 mM of manganese(II) acetylacetonate and 0.05 mM of gold(III) acetate (20:1 $Mn(acac)_2/Au(OOCCH_3)_3$) placed in a glovebox. The resulting mixture was rapidly heated to 265 °C with vigorous stirring. After refluxing for 60 min, the mixture was allowed to cool to room temperature under argon flow. Ethanol was added to the mixture to precipitate a dark-purple product, which was collected by centrifuging at 10 000 rpm for 15 min. The precipitated product was redispersed in toluene or hexane and reprecipitated by addition of ethanol. This purification process was repeated three times. Finally, the product was dissolved in toluene or hexane, flushed with argon, and stored at 4 °C for further use.

Transfer of Au@MnO Nanoflowers into Aqueous Phase. Aqueous phase transfer of Au@MnO nanoflowers from toluene or hexane to ultrapure water or PBS buffer was achieved using heterobifunctional ligand (see Suppoting Information Scheme S1 for structure and synthesis).[77] The hydroxyl (OH) groups on the dopamine side of the PEG ligand preferentially bind the surface of the MnO domain of nanoflowers, and the carboxyl group on the other side contributes water solubility and is free to react with aptamers in the presence of 1-ethyl-3-(3-dimethylaminopropyl)-carbodiimide), EDC, and *N*-hydroxysulfosuccinimide (Sulfo-NHS).

A 10 mg sample of Au@MnO nanoflowers was dissolved in 5 mL of anhydrous terahydrofuran (THF) and flushed with argon

for 15 min. After degassing, the solution was transferred to a dropping funnel. Heterobifunctional dopamine-terminated PEG (150 mg) was dissolved in 20 mL of anhydrous THF in a 100 mL three-necked flask. The nanoflower solution was added dropwise to the PEG ligand solution. The resultant mixture was stirred under argon for 15 min and kept under an argon blanket at 50 °C overnight. The nanoflower−PEG conjugates were precipitated *via* addition of ~3 mL of hexane and collected by centrifugation at 10 000 rpm for 20 min. The supernatant was discarded, and the product, a nanoflower−PEG conjugate at the bottom of the centrifuge tube, was washed with ethanol and centrifuged twice to remove excess unreacted PEG ligands. Finally, the nanoflower precipitate was dispersed in 2 mL of ultrapure water or PBS buffer for aptamer conjugation.

Functionalization of Au@MnO Nanoflowers. Conventional protein labeling chemistry was utilized to attach two different aptamers, sgc8 and anti-ATP, to the surfaces of two different nanoflower domains, MnO and Au. A 30 μL aliquot of 0.1 M 1-ethyl-3-(3-dimethylaminopropyl)carbodiimide (EDC) was added to 150 μg/mL nanoflowers in 10 mM phosphate buffered saline (PBS) to activate the carboxyl group on the PEG ligand for 20 min. After gently shaking for 20 min, 13.1 μL of 228 μM sgc8 aptamer and 30 μL of 0.12 M *N*-hydroxysuccinimide (NHS) in 10 mM PBS buffer were added and incubated for 1 h, while gently shaking to functionalize the MnO domain of nanoflowers. After 1 h incubation, 7.45 μL of 300 μM anti-ATP aptamer and 77 μL of 10 mM PBS buffer were added, and the mixture was placed on a shaker for incubation overnight at room temperature to functionalize the Au domain. Before immobilization of the anti-ATP aptamer, the thiol modified on the 5′-end was deprotected by dithiothreitol (DTT). One millimolar 5′-thiol-modified anti-ATP aptamer in 1 mL of 10 mM PBS buffer (pH 8.3) was incubated with 1 M DTT for 30 min at room temperature to deprotect the thiol functionality. Excess DTT was removed by washing five times with 0.5 mL of ethylacetate. After immobilization of aptamers onto nanoflowers, the resultant mixture was washed three times with 10 mM PBS buffer and finally redispersed in 300 μL of 10 mM PBS buffer.

Conflict of Interest: The authors declare no competing financial interest.

Acknowledgment. This work is supported by grants awarded by the National Institutes of Health (GM066137, GM079359 and CA133086), by the National Key Scientific Program of China (2011CB911000), NSFC (Grant 21221003) and China National Instrumentation Program 2011YQ03012412. We thank K. N. Siebein at the Major Analytical Instrumentation Center at the University of Florida for assistance with HR-TEM measurements. We also sincerely appreciate Dr. K. Williams for assistance with manuscript revision. We thank for the summer fellowship support from Eastman Chemical Company to B.G. We acknowledge the Ministry of National Education, Republic of Turkey, for financial support to I.O. with full fellowship during his Ph.D. at the University of Florida.

Supporting Information Available: Three-step synthesis of the heterobifunctional dopamine-PEG-COOH ligand and synthesis details of hybrid nanoparticles, Fe_3O_4@Au core−shell, Au-Fe_3O_4 dimer, Au@Fe_3O_4 nanoflowers. TEM images, UV−vis spectra of nanoparticles. Synthesis of benzylpyridinium salt (BP) for survival yield experiments and survival yield calculation on hybrid nanoparticles. Testing Au@MnO nanoflowers as a matrix for laser desorption ionization with different biomolecules. This material is available free of charge *via* the Internet at http://pubs.acs.org.

REFERENCES AND NOTES

1. Ma, X.; Zhao, Y.; Liang, X.-J. Theranostic Nanoparticles Engineered for Clinic and Pharmaceutics. *Acc. Chem. Res.* **2011**, *44*, 1114–1122.
2. Wang, H.; Yang, R.; Yang, L.; Tan, W. Nucleic Acid Conjugated Nanomaterials for Enhanced Molecular Recognition. *ACS Nano* **2009**, *3*, 2451–2460.
3. Hu, R.; Zhang, X.-B.; Kong, R.-M.; Zhao, X.-H.; Jiang, J.; Tan, W. Nucleic Acid-Functionalized Nanomaterials for Bioimaging Applications. *J. Mater. Chem.* **2011**, *21*, 16323–16334.
4. Jain, P. K.; Huang, X.; El-Sayed, I. H.; El-Sayed, M. A. Noble Metals on the Nanoscale: Optical and Photothermal Properties and Some Applications in Imaging, Sensing, Biology, and Medicine. *Acc. Chem. Res.* **2008**, *41*, 1578–1586.
5. Dreaden, E. C.; Mackey, M. A.; Huang, X.; Kang, B.; El-Sayed, M. A. Beating Cancer in Multiple Ways Using Nanogold. *Chem. Soc. Rev.* **2011**, *40*, 3391–3404.
6. Dreaden, E. C.; Alkilany, A. M.; Huang, X.; Murphy, C. J.; El-Sayed, M. A. The Golden Age: Gold Nanoparticles for Biomedicine. *Chem. Soc. Rev.* **2012**, *41*, 2740–2779.
7. Veiseh, O.; Gunn, J. W.; Zhang, M. Design and Fabrication of Magnetic Nanoparticles for Targeted Drug Delivery and Imaging. *Adv. Drug Delivery Rev.* **2010**, *62*, 284–304.
8. Sun, C.; Lee, J. S. H.; Zhang, M. Magnetic Nanoparticles in MR Imaging and Drug Delivery. *Adv. Drug Delivery Rev.* **2008**, *60*, 1252–1265.
9. Gao, J.; Gu, H.; Xu, B. Multifunctional Magnetic Nanoparticles: Design, Synthesis, and Biomedical Applications. *Acc. Chem. Res.* **2009**, *42*, 1097–1107.
10. Das, M.; Mishra, D.; Dhak, P.; Gupta, S.; Maiti, T. K.; Basak, A.; Pramanik, P. Biofunctionalized, Phosphonate-Grafted, Ultrasmall Iron Oxide Nanoparticles for Combined Targeted Cancer Therapy and Multimodal Imaging. *Small* **2009**, *5*, 2883–2893.
11. Pan, D.; Caruthers, S. D.; Hu, G.; Senpan, A.; Scott, M. J.; Gaffney, P. J.; Wickline, S. A.; Lanza, G. M. Ligand-Directed Nanobialys as Theranostic Agent for Drug Delivery and Manganese-Based Magnetic Resonance Imaging of Vascular Targets. *J. Am. Chem. Soc.* **2008**, *130*, 9186–9187.
12. Bae, K. H.; Lee, K.; Kim, C.; Park, T. G. Surface Functionalized Hollow Manganese Oxide Nanoparticles for Cancer Targeted SiRNA Delivery and Magnetic Resonance Imaging. *Biomaterials* **2011**, *32*, 176–184.
13. Kim, J.; Park, S.; Lee, J. E.; Jin, S. M.; Lee, J. H.; Lee, I. S.; Yang, I.; Kim, J.-S.; Kim, S. K.; Cho, M.-H.; *et al.* Designed Fabrication of Multifunctional Magnetic Gold Nanoshells and Their Application to Magnetic Resonance Imaging and Photothermal Therapy. *Angew. Chem., Int. Ed.* **2006**, *118*, 7918–7922.
14. Hirsch, L. R.; Stafford, R. J.; Bankson, J. A.; Sershen, S. R.; Rivera, B.; Price, R. E.; Hazle, J. D.; Halas, N. J.; West, J. L. Nanoshell-Mediated Near-Infrared Thermal Therapy of Tumors under Magnetic Resonance Guidance. *Proc. Natl. Acad. Sci. U.S.A.* **2003**, *100*, 13549–13554.
15. Sanvicens, N.; Marco, M. P. Multifunctional Nanoparticles—Properties and Prospects for Their Use in Human Medicine. *Trends Biotechnol.* **2008**, *26*, 425–433.
16. Lee, D.-E.; Koo, H.; Sun, I.-C.; Ryu, J. H.; Kim, K.; Kwon, I. C. Multifunctional Nanoparticles for Multimodal Imaging and Theragnosis. *Chem. Soc. Rev.* **2012**, *41*, 2656–2672.
17. Yu, H.; Chen, M.; Rice, P. M.; Wang, S. X.; White, R. L.; Sun, S. Dumbbell-like Bifunctional Au-Fe_3O_4 Nanoparticles. *Nano Lett.* **2005**, *5*, 379–382.
18. Xu, C.; Xie, J.; Ho, D.; Wang, C.; Kohler, N.; Walsh, E. G.; Morgan, J. R.; Chin, Y. E.; Sun, S. Au-Fe_3O_4 Dumbbell Nanoparticles as Dual-Functional Probes. *Angew. Chem., Int. Ed.* **2008**, *47*, 173–176.
19. Lee, Y.; Garcia, M. A.; Frey Huls, N. A.; Sun, S. Synthetic Tuning of the Catalytic Properties of Au-Fe_3O_4 Nanoparticles. *Angew. Chem., Int. Ed.* **2010**, *49*, 1271–1274.
20. Xie, J.; Zhang, F.; Aronova, M.; Zhu, L.; Lin, X.; Quan, Q.; Liu, G.; Zhang, G.; Choi, K.-Y.; Kim, K.; *et al.* Manipulating the Power of an Additional Phase: A Flower-like Au-Fe_3O_4 Optical Nanosensor for Imaging Protease Expressions *in Vivo*. *ACS Nano* **2011**, *5*, 3043–3051.
21. Schladt, T. D.; Shukoor, M. I.; Schneider, K.; Tahir, M. N.; Natalio, F.; Ament, I.; Becker, J.; Jochum, F. D.; Weber, S.; Köhler, O.; *et al.* Au@MnO Nanoflowers: Hybrid Nanocomposites for Selective Dual Functionalization and Imaging. *Angew. Chem., Int. Ed.* **2010**, *49*, 3976–3980.
22. Song, H.-M.; Wei, Q.; Ong, Q. K.; Wei, A. Plasmon-Resonant Nanoparticles and Nanostars with Magnetic Cores: Synthesis and Magnetomotive Imaging. *ACS Nano* **2010**, *4*, 5163–5173.
23. Lu, J.; Wang, M.; Li, Y.; Deng, C. Facile Synthesis of TiO_2/Graphene Composites for Selective Enrichment of Phosphopeptides. *Nanoscale* **2012**, *4*, 1577–1580.

24. Zenobi, R.; Knochenmuss, R. Ion Formation in MALDI Mass Spectrometry. *Mass Spectrom. Rev.* **1998**, *17*, 337–366.
25. Knochenmuss, R. Ion Formation Mechanisms in UV-MALDI. *Analyst* **2006**, *131*, 966–986.
26. Chiang, C.-K.; Chen, W.-T.; Chang, H.-T. Nanoparticle-Based Mass Spectrometry for the Analysis of Biomolecules. *Chem. Soc. Rev.* **2011**, *40*, 1269–1281.
27. Tanaka, K.; Waki, H.; Ido, Y.; Akita, S.; Yoshida, Y.; Yoshida, T.; Matsuo, T. Protein and Polymer Analyses up to *m/z* 100000 by Laser Ionization Time-of-Flight Mass Spectrometry. *Rapid Commun. Mass Spectrom.* **1988**, *2*, 151–153.
28. Harkness, K. M.; Cliffel, D. E.; McLean, J. A. Characterization of Thiolate-Protected Gold Nanoparticles by Mass Spectrometry. *Analyst* **2010**, *135*, 868–874.
29. Zhu, Z.-J.; Rotello, V. M.; Vachet, R. W. Engineered Nanoparticle Surfaces for Improved Mass Spectrometric Analyses. *Analyst* **2009**, *134*, 2183–2188.
30. Yan, B.; Zhu, Z.-J.; Miranda, O.; Chompoosor, A.; Rotello, V.; Vachet, R. Laser Desorption/Ionization Mass Spectrometry Analysis of Monolayer-Protected Gold Nanoparticles. *Anal. Bioanal. Chem.* **2010**, *396*, 1025–1035.
31. Dass, A.; Stevenson, A.; Dubay, G. R.; Tracy, J. B.; Murray, R. W. Nanoparticle MALDI-TOF Mass Spectrometry without Fragmentation: $Au_{25}(SCH_2CH_2Ph)_{18}$ and Mixed Monolayer $Au_{25}(SCH_2CH_2Ph)_{18-x}(L)_x$. *J. Am. Chem. Soc.* **2008**, *130*, 5940–5946.
32. Tang, J.; Liu, Y.; Qi, D.; Yao, G.; Deng, C.; Zhang, X. On-Plate-Selective Enrichment of Glycopeptides Using Boronic Acid-Modified Gold Nanoparticles for Direct MALDI-QIT-TOF MS Analysis. *Proteomics* **2009**, *9*, 5046–5055.
33. Huang, Y.-F.; Chang, H.-T. Analysis of Adenosine Triphosphate and Glutathione through Gold Nanoparticles Assisted Laser Desorption/Ionization Mass Spectrometry. *Anal. Chem.* **2007**, *79*, 4852–4859.
34. Shrivas, K.; Wu, H.-F. Multifunctional Nanoparticles Composite for MALDI-MS: Cd^{2+}-Doped Carbon Nanotubes with CdS Nanoparticles as the Matrix, Preconcentrating and Accelerating Probes of Microwave Enzymatic Digestion of Peptides and Proteins for Direct MALDI-MS Analysis. *J. Mass Spectrom.* **2010**, *45*, 1452–1460.
35. Chang, S.; Zheng, N.-Y.; Chen, C.-S.; Chen, C.-D.; Chen, Y.-Y.; Wang, C. Analysis of Peptides and Proteins Affinity-Bound to Iron Oxide Nanoparticles by MALDI MS. *J. Am. Soc. Mass. Spectrom.* **2007**, *18*, 910–918.
36. Chiang, C.-K.; Chiang, M.-C.; Lin, Z.-H.; Lan, G.-Y.; Lin, Y.-W.; Chang, H.-T. Nanomaterial-Based Surface-Assisted Laser Desorption/Ionization Mass Spectrometry of Peptides and Proteins. *J. Am. Soc. Mass. Spectrom.* **2010**, *21*, 1204–1207.
37. Gulbakan, B.; Yasun, E.; Shukoor, M. I.; Zhu, Z.; You, M.; Tan, X.; Sanchez, H.; Powell, D. H.; Dai, H.; Tan, W. A Dual Platform for Selective Analyte Enrichment and Ionization in Mass Spectrometry Using Aptamer-Conjugated Graphene Oxide. *J. Am. Chem. Soc.* **2010**, *132*, 17408–17410.
38. Gulbakan, B.; Park, D.; Kang, M.; Kececi, K.; Martin, C. R.; Powell, D. H.; Tan, W. Laser Desorption Ionization Mass Spectrometry on Silicon Nanowell Arrays. *Anal. Chem.* **2010**, *82*, 7566–7575.
39. Chiang, C.-K.; Yang, Z.; Lin, Y.-W.; Chen, W.-T.; Lin, H.-J.; Chang, H.-T. Detection of Proteins and Protein−Ligand Complexes Using HgTe Nanostructure Matrixes in Surface-Assisted Laser Desorption/Ionization Mass Spectrometry. *Anal. Chem.* **2010**, *82*, 4543–4550.
40. Zhu, Z.-J.; Tang, R.; Yeh, Y.-C.; Miranda, O. R.; Rotello, V. M.; Vachet, R. W. Determination of the Intracellular Stability of Gold Nanoparticle Monolayers Using Mass Spectrometry. *Anal. Chem.* **2012**, *84*, 4321–4326.
41. Creran, B.; Yan, B.; Moyano, D. F.; Gilbert, M. M.; Vachet, R. W.; Rotello, V. M. Laser Desorption Ionization Mass Spectrometric Imaging of Mass Barcoded Gold Nanoparticles for Security Applications. *Chem. Commun.* **2012**, *48*, 4543–4545.
42. Zhu, Z.-J.; Ghosh, P. S.; Miranda, O. R.; Vachet, R. W.; Rotello, V. M. Multiplexed Screening of Cellular Uptake of Gold Nanoparticles Using Laser Desorption/Ionization Mass Spectrometry. *J. Am. Chem. Soc.* **2008**, *130*, 14139–14143.
43. Meng, J.-c.; Siuzdak, G.; Finn, M. G. Affinity Mass Spectrometry from a Tailored Porous Silicon Surface. *Chem. Commun.* **2004**, 2108–2109.
44. Lowe, R. D.; Szili, E. J.; Kirkbride, P.; Thissen, H.; Siuzdak, G.; Voelcker, N. H. Combined Immunocapture and Laser Desorption/Ionization Mass Spectrometry on Porous Silicon. *Anal. Chem.* **2010**, *82*, 4201–4208.
45. Kausaite-Minkstimiene, A.; Ramanaviciene, A.; Kirlyte, J.; Ramanavicius, A. Comparative Study of Random and Oriented Antibody Immobilization Techniques on the Binding Capacity of Immunosensor. *Anal. Chem.* **2010**, *82*, 6401–6408.
46. Tajima, N.; Takai, M.; Ishihara, K. Significance of Antibody Orientation Unraveled: Well-Oriented Antibodies Recorded High Binding Affinity. *Anal. Chem.* **2011**, *83*, 1969–1976.
47. Alves, N. J.; Kiziltepe, T.; Bilgicer, B. Oriented Surface Immobilization of Antibodies at the Conserved Nucleotide Binding Site for Enhanced Antigen Detection. *Langmuir* **2012**, *28*, 9640–9648.
48. Song, H. Y.; Zhou, X.; Hobley, J.; Su, X. Comparative Study of Random and Oriented Antibody Immobilization As Measured by Dual Polarization Interferometry and Surface Plasmon Resonance Spectroscopy. *Langmuir* **2011**, *28*, 997–1004.
49. Tang, Z.; Shangguan, D.; Wang, K.; Shi, H.; Sefah, K.; Mallikratchy, P.; Chen, H. W.; Li, Y.; Tan, W. Selection of Aptamers for Molecular Recognition and Characterization of Cancer Cells. *Anal. Chem.* **2007**, *79*, 4900–4907.
50. Shangguan, D.; Cao, Z.; Meng, L.; Mallikaratchy, P.; Sefah, K.; Wang, H.; Li, Y.; Tan, W. Cell-Specific Aptamer Probes for Membrane Protein Elucidation in Cancer Cells. *J. Proteome Res.* **2008**, *7*, 2133–2139.
51. Shangguan, D.; Li, Y.; Tang, Z.; Cao, Z. C.; Chen, H. W.; Mallikaratchy, P.; Sefah, K.; Yang, C. J.; Tan, W. Aptamers Evolved From Live Cells as Effective Molecular Probes for Cancer Study. *Proc. Natl. Acad. Sci. U.S.A.* **2006**, *103*, 11838–11843.
52. Zhou, X.; Duan, R.; Xing, D. Highly Sensitive Detection of Protein and Small Molecules Based on Aptamer-Modified Electrochemiluminescence Nanoprobe. *Analyst* **2012**, *137*, 1963–1969.
53. Liu, J.; Lu, Y. Fast Colorimetric Sensing of Adenosine and Cocaine Based on a General Sensor Design Involving Aptamers and Nanoparticles. *Angew. Chem., Int. Ed.* **2006**, *45*, 90–94.
54. Miao, X.; Ling, L.; Shuai, X. Ultrasensitive Detection of Lead(II) with DNAzyme and Gold Nanoparticles Probes by Using a Dynamic Light Scattering Technique. *Chem. Commun.* **2011**, *47*, 4192–4194.
55. Lin, Y.-W.; Liu, C.-W.; Chang, H.-T. Fluorescence Detection of Mercury(II) and Lead(II) Ions Using Aptamer/Reporter Conjugates. *Talanta* **2011**, *84*, 324–329.
56. Rotem, D.; Jayasinghe, L.; Salichou, M.; Bayley, H. Protein Detection by Nanopores Equipped with Aptamers. *J. Am. Chem. Soc.* **2012**, *134*, 2781–2787.
57. Wang, J.; Zhu, G.; You, M.; Song, E.; Shukoor, M. I.; Zhang, K.; Altman, M. B.; Chen, Y.; Zhu, Z.; Huang, C. Z.; *et al.* Assembly of Aptamer Switch Probes and Photosensitizer on Gold Nanorods for Targeted Photothermal and Photodynamic Cancer Therapy. *ACS Nano* **2012**, *6*, 5070–5077.
58. Yasun, E.; Gulbakan, B.; Ocsoy, I.; Yuan, Q.; Shukoor, M. I.; Li, C.; Tan, W. Enrichment and Detection of Rare Proteins with Aptamer-Conjugated Gold Nanorods. *Anal. Chem.* **2012**, *84*, 6008–6015.
59. Bamrungsap, S.; Chen, T.; Shukoor, M. I.; Chen, Z.; Sefah, K.; Chen, Y.; Tan, W. Pattern Recognition of Cancer Cells Using Aptamer-Conjugated Magnetic Nanoparticles. *ACS Nano* **2012**, *6*, 3974–3981.
60. Chen, T.; Shukoor, M. I.; Chen, Y.; Yuan, Q.; Zhu, Z.; Zhao, Z.; Gulbakan, B.; Tan, W. Aptamer-Conjugated Nanomaterials for Bioanalysis and Biotechnology Applications. *Nanoscale* **2011**, *3*, 546–556.
61. Fan, Z.; Shelton, M.; Singh, A. K.; Senapati, D.; Khan, S. A.; Ray, P. C. Multifunctional Plasmonic Shell−Magnetic Core Nanoparticles for Targeted Diagnostics, Isolation, and

Photothermal Destruction of Tumor Cells. *ACS Nano* **2012**, *6*, 1065–1073.
62. Kim, Y.-K.; Na, H.-K.; Kwack, S.-J.; Ryoo, S.-R.; Lee, Y.; Hong, S.; Hong, S.; Jeong, Y.; Min, D.-H. Synergistic Effect of Graphene Oxide/MWCNT Films in Laser Desorption/Ionization Mass Spectrometry of Small Molecules and Tissue Imaging. *ACS Nano* **2011**, *5*, 4550–4561.
63. Kim, Y.-K.; Min, D.-H. Preparation of the Hybrid Film of Poly(allylamine hydrochloride)-Functionalized Graphene Oxide and Gold Nanoparticle and Its Application for Laser-Induced Desorption/Ionization of Small Molecules. *Langmuir* **2012**, *28*, 4453–4458.
64. Kim, Y.-K.; Min, D.-H. Fabrication of Alternating Multilayer Films of Graphene Oxide and Carbon Nanotube and Its Application in Mechanistic Study of Laser Desorption/Ionization of Small Molecules. *ACS Appl. Mater. Interfaces* **2012**, *4*, 2088–2095.
65. Sellick, C. A.; Hansen, R.; Stephens, G. M.; Goodacre, R.; Dickson, A. J. Metabolite Extraction from Suspension-Cultured Mammalian Cells for Global Metabolite Profiling. *Nat. Protoc.* **2011**, *6*, 1241–1249.
66. Chen, Y.; O'Donoghue, M. B.; Huang, Y.-F.; Kang, H.; Phillips, J. A.; Chen, X.; Estevez, M. C.; Yang, C. J.; Tan, W. A Surface Energy Transfer Nanoruler for Measuring Binding Site Distances on Live Cell Surfaces. *J. Am. Chem. Soc.* **2010**, *132*, 16559–16570.
67. Yanes, O.; Tautenhahn, R.; Patti, G. J.; Siuzdak, G. Expanding Coverage of the Metabolome for Global Metabolite Profiling. *Anal. Chem.* **2011**, *83*, 2152–2161.
68. Cutler, J. I.; Auyeung, E.; Mirkin, C. A. Spherical Nucleic Acids. *J. Am. Chem. Soc.* **2012**, *134*, 1376–1391.
69. Seferos, D. S.; Giljohann, D. A.; Hill, H. D.; Prigodich, A. E.; Mirkin, C. A. Nano-Flares: Probes for Transfection and mRNA Detection in Living Cells. *J. Am. Chem. Soc.* **2007**, *129*, 15477–15479.
70. Wang, Y.; Li, Z.; Hu, D.; Lin, C.-T.; Li, J.; Lin, Y. Aptamer/Graphene Oxide Nanocomplex for *In Situ* Molecular Probing in Living Cells. *J. Am. Chem. Soc.* **2010**, *132*, 9274–9276.
71. Tan, X.; Chen, T.; Xiong, X.; Mao, Y.; Zhu, G.; Yasun, E.; Li, C.; Zhu, Z.; Tan, W. Semiquantification of ATP in Live Cells Using Nonspecific Desorption of DNA from Graphene Oxide as the Internal Reference. *Anal. Chem.* **2012**, *84*, 8622–8627.
72. Tan, X.; Chen, W.; Lu, S.; Zhu, Z.; Chen, T.; Zhu, G.; You, M.; Tan, W. Molecular Beacon Aptamers for Direct and Universal Quantitation of Recombinant Proteins from Cell Lysates. *Anal. Chem.* **2012**, *84*, 8272–8276.
73. Zheng, D.; Seferos, D. S.; Giljohann, D. A.; Patel, P. C.; Mirkin, C. A. Aptamer Nano-Flares for Molecular Detection in Living Cells. *Nano Lett.* **2009**, *9*, 3258–3261.
74. Sellick, C. A.; Hansen, R.; Maqsood, A. R.; Dunn, W. B.; Stephens, G. M.; Goodacre, R.; Dickson, A. J. Effective Quenching Processes for Physiologically Valid Metabolite Profiling of Suspension Cultured Mammalian Cells. *Anal. Chem.* **2008**, *81*, 174–183.
75. El-Serag, H. B. Hepatocellular Carcinoma. *N. Engl. J. Med.* **2011**, *365*, 1118–1127.
76. Villanueva, A.; Minguez, B.; Forner, A.; Reig, M.; Llovet, J. M. Hepatocellular Carcinoma: Novel Molecular Approaches for Diagnosis, Prognosis, and Therapy. *Annu. Rev. Med.* **2010**, *61*, 317–328.
77. Chen, T.; Shukoor, M. I.; Wang, R.; Zhao, Z.; Yuan, Q.; Bamrungsap, S.; Xiong, X.; Tan, W. Smart Multifunctional Nanostructure for Targeted Cancer Chemotherapy and Magnetic Resonance Imaging. *ACS Nano* **2011**, *5*, 7866–7873.